IEEE Access
Multidisciplinary | Rapid Review | Open Access Journal

Received May 10, 2021, accepted May 25, 2021, date of publication June 3, 2021, date of current version June 16, 2021.

*Digital Object Identifier 10.1109/ACCESS.2021.3085976*

# Simplex Search Method Driven Design for Transient Stability Enhancement in Wind Energy Integrated Power System Using Multi-Band PSS4C

**AHMAD ADEL ALSAKATI[1], (Student Member, IEEE), CHOCKALINGAM ARAVIND VAITHILINGAM[1], (Senior Member, IEEE), JAMAL ALNASSEIR[2], AND ARTHANARI JAGADEESHWARAN[3], (Member, IEEE)**

[1]High Impact Research Laboratory, Faculty of Innovation and Technology, School of Computer Science and Engineering, Taylor's University at Lakeside, Subang Jaya 47500, Malaysia
[2]Electric Power Engineering Department, Faculty of Mechanical and Electrical Engineering, Damascus University, Damascus, Syria
[3]Department of Electrical and Electronics Engineering, Sona College of Technology, Salem 636005, India

Corresponding author: Jamal Alnasseir (jamalnasseir@yahoo.de)

This work was supported by Taylor's University through its Taylor's Research Scholarship Programme under Grant TUFR/2017/001/01.

**ABSTRACT** Wind Energy serves as one of the most cost-efficient renewable sources of energy that reduces the carbon emissions. The need for stability enhancement in power systems with the integration of wind energy is a great concern as this is future forward towards energy sustainability. Multi-Band Power System Stabilizer (MB-PSS) has proven to be an effective controller to increase the efficiency and stability of power systems. This article presents a novel method for MB-PSS4C optimization under the fault condition, where the parameters are tuned based on the Simplex Search method. The wind energy integrated power system is investigated to assess the effect of wind energy uncertainty on transient stability and an in-depth analysis of actual wind speed is conducted. A 3-phase fault is carried out to evaluate the effect of Optimized OMB-PSS4C on the stability of two-area four-machine system integrated with wind energy. MATLAB is used to investigate transient stability based on the nonlinear simulation of relative power angle and speed deviation of synchronous generators (SGs). The presented results established that when the OMB-PSS4C and exciter ST1A are used, the relative power angle changed from an unstable to steady-state within the settling time of around 3 s with an accompanying decrease of peak value from 54.8° to 43.23°. The high penetration of wind energy has the potential to cause an increase in settling time, for instance the settling time increased to 7.87 s after integrating 108 MW based wind energy. However, the stability of the system is guaranteed with the utilization of OMB-PSS4C.

**INDEX TERMS** Doubly Fed Induction Generator (DFIG), Multi-Band Power System Stabilizer MB-PSS4C, Simplex Search, transient stability, wind energy.

## I. INTRODUCTION

The utilization of renewable energies is significantly growing due to the decline of fossil fuel resource, an increase in global energy demand and the negative environmental consequences of fossil fuels. Renewable energy, such as photovoltaic and wind energy are considered alternative solutions to address climate change associated to the above concerns [1], [2]. Wind energy is one of the most promising sources for clean electricity generation and plays a vital role in reducing carbon-related emissions [3]. Doubly Fed Induction Generators (DFIGs) is a common design due to its efficiency and the ability to control the reactive power [4] with the stator connected to the grid. The rotor is driven by a converter, which controls voltage and frequency as required by the grid [5].

The penetration of wind energy into electrical networks has increased worldwide, but the characteristics of wind turbines differ from conventional power plants [6] and performance of converter-based resources varies from the systems used in SGs [7]. Therefore, the high penetration level of wind energy raises a great concern of its effects on the behaviour of the grid. The output power of wind energy is not as stable as power plants, and the grid is expected to withstand and

The associate editor coordinating the review of this manuscript and approving it for publication was Ton Duc Do.

This work is licensed under a Creative Commons Attribution-NonCommercial-NoDerivatives 4.0 License.
For more information, see https://creativecommons.org/licenses/by-nc-nd/4.0/

ensure power stability of the wind energy system. The high penetration of wind energy creates some challenges leading to significant changes of the existing power system, and affects the stability of integrated power system with wind energy [1], [4], [6]–[9].

Transient stability is a critical issue in power system reliability and efficiency, and represents the capability of a power system to remain synchronized after a large disturbance [6], [10]. Flexible AC transmission systems [11], static synchronous compensator [12]–[15], static VAR compensator [14], [16], and static series synchronous compensator [17] are some techniques used to improve the stability of power systems. However, Power System Stabilizer (PSS) is considered more of an efficient controller and cost-effective solution to dampen the oscillations [18], [19]. Large power systems pull several oscillation modes depending on their structure and size [5]. PSS is designed to cope with local, inter-area, and global modes of oscillations. The local mode refers to a generator swinging against the power system. In contrast, the inter-area mode refers to the swinging of generators against each other in diverse areas or locations [20]. Global mode is indicated by the imbalance between load and generation [19].

Multi-Band Power System Stabilizer (MB-PSS) contains multiple bands being low, intermediate, and high bands associated with global, inter-area and local modes. MB-PSS has more advantages in comparison to conventional PSS in the mode damping of oscillations [19], [21]. The development of MB-PSS is targeted to address the oscillation modes, the nonlinearity and uncertainty associated with modern power systems, owing to variable wind energy integration. A conventional MB-PSS may not ensure the optimal solution since its parameters are constant, and the power system is nonlinear. If the parameters of conventional MB-PSS are not carefully selected, it can induce changes to power system stability. Therefore, the selection of MB-PSS parameters is made with utmost carefulness based on the excitation system and the network structure.

This work focusses on the enhancement of transient stability of power system with wind energy based on the application of Optimized OMB-PSS4C. The four-machine two-area system integrated wind energy is considered under large disturbances. The performance of OMB-PSS4C is compared with PSS1A (the parameters of PSS1A are chosen based on IEEE Standard) to validate the proposed method for tuning the parameters of OMB-PSS4C. The nonlinear simulations are analysed to evaluate the efficiency of PSS. The relative power angle [4], [7]–[9], speed or (speed deviation) [17], [22], voltage, and electrical power [5] of Synchronous Generators (SGs) are used in stability evaluation of modern power system. Equally considered with the fault condition during PSS tuning process through the MB-PSS4C optimization. The contributions of this article compared with other research works in this area are summarized as stated below:

(1) Optimization of MB-PSS4C parameters based on Pattern Search and Simplex Search methods.
(2) A novel method is proposed to tune the parameters of MB-PSS4C under fault condition.
(3) The application of OMB-PSS4C for transient stability enhancement of power system integrated wind energy with different penetration levels.

This article is structured as follows; Section 2 summarizes some literature related to this topic. The wind data, power system stabilizers and formulation of optimization methods are analysed and described in Section 3. In Section 4, the results of studied system and discussion are presented. Finally, the conclusion is discussed in the last section.

## II. LITERATURE REVIEW

Different types of PSSs, including PSS2B, and PSS4B, were investigated in [23]. Authors concluded that both PSSs have a similar response in local and intra-unit, but PSS4B has the better response in inter-area mode. Ref. [24] designed the multiple PSSs in two-area four-machine and 39-bus systems based on eigenvalue stability and nonlinearity indexes. The single-input PSS and dual-input PSS2B were investigated. The simulation results proved the advantages of using stability-nonlinearity index-based PSS design by hyper-spherical search. Moreover, PSS2B offered better improvements in comparison to the single-input PSS. Rimorov *et al.* [19] investigated the single-input PSS1A and PSS4B for damping low frequency oscillations. The improved modal performance index was used in PSS4B parameter optimization, and the conventional method employed in the design of PSS1A. It was established that PSS4B has greater efficiency in damping global, inter-area, and local modes compared to PSS1A.

Hybrid Particle Swarm Optimization has been implemented to tune PSS4B parameters using two steps [25]. The hybrid blocks and gains were optimized in the first step, and lead-lag blocks were determined in the second step. The performance of the tuning method was compared with the general technique. The results proved the superiority of this method to suppress the oscillations. Another combination of three hybrid methods, gravitational search algorithm, bat algorithm and PSO, proposed in [26] to enhance the optimization process of MB PSS4B. The optimization method was applied to maximize the damping ratio coefficient of multi-machine power systems. Authors concluded that the proposed method improves the global search capability as well as the fast convergence of their method to perform a local search. In another study, Peres *et al.* [27] applied a pole placement method to adjust simplified MB-PSS gains and maximise the damping ratio. A single-machine infinite bus and multi-machine power systems were used to validate the method under various operating conditions; it was concluded that a low computational process was required when compared with other conventional techniques. While these studies mainly focused on PSS4B, Li *et al.* [28] applied PSS4C

to improve the stability of a 9-bus system integrated with photovoltaic and wind turbine. The PSS4C showed better performance in mitigating very low-frequency oscillations compared with other designs.

Various strategies were adopted in the design of PSS for two-area four-machine system integrated wind energy. Uncertainty in the power system with 300 MW generated by wind energy was investigated [22]. The optimized fuzzy PSS was proposed to improve dynamic stability and decrease uncertainties associated with generators, transmission lines, and load demand. Settling time, first-swing and back-swing amplitudes were considered to assess the stability of power system. The proposed controller showed good performance during the 200 ms fault under different conditions. The effect of wind energy on power systems was investigated in [8], and the SGs were replaced by DFIGs with the same power. The eigenvalue was used to evaluate the small-signal stability of 39-bus system under different conditions. The authors concluded that the wind turbines worsened the instability. However, SG control systems (automatic voltage regulator and PSS), improved stability and dampened the oscillations.

Eigenvalue analysis was used to study the impacts of DFIG, the penetration, and its location on the oscillations of two-area four-machine systems with PSS [4]. The results showed that the high penetration of DFIG has a very significant impact on oscillation modes, particularly the inter-area mode. Moreover, the oscillations were mitigated with the integration of PSS. The chaotic PSO Passive Congregation was utilized to optimize PSS for a two-area four-machine system integrated wind energy [5]. Eigenvalue and damping ratio were considered as objective functions for the optimization problem. The nonlinear simulations demonstrated the efficiency of the proposed algorithm in the design of PSS and stability improvement of the power system integrated wind turbines. A summary of the above-mentioned literature review is presented in Table 1, based on different types of PSSs and tuning methods.

As observed in Table 1, eigenvalue analysis and damping ratio are common methods in application for PSS tuning parameters [4], [5], [8]. These methods are used in the linearization of power system through a small-signal stability analysis under different operating conditions and through providing accurate approximation over small disturbances. However, the power system remains nonlinear in nature, making it difficult to achieve a linearized model for a large system. Furthermore, the integration of DFIG in the power system promotes the nonlinearity of the system. Therefore, the linearized model may not represent the stability status [5]. In this research, an effective method is utilized to optimize MB-PSS4C parameters under large disturbance without applying the approximate techniques to obtain the linear systems.

In the literature mentioned above, several studies discussed the good performance of MB-PSS4B with suitable tuning methods. Nevertheless, few studies highlighted MB-PSS4C's

**TABLE 1. Summary of the existing literature review and comparison with our proposed work.**

| Ref. | Type of controller | Optimization technique | Remarks |
|---|---|---|---|
| He et al. (2016) [4] | PSS | Eigenvalue analysis | Evaluate the impact of DFIG on low frequency oscillations. |
| Nakhi and Kamarposhti (2019) [22] | PSS | Optimized fuzzy PSS | Uncertainty in the power system with wind energy is analyzed. The effect of different wind energy penetrations is not evaluated. |
| Derafshian and Amjady (2015) [5] | PSS | chaotic PSO passive congregation | Eigenvalue and time-domain simulations are used to evaluate the proposed method |
| Essallah, Bouallegue and Khedher (2018) [8] | automatic voltage regulator and PSS | Eigenvalue analysis | Eigenvalue is used to evaluate small-signal stability. |
| Rimorov, Kamwa and Joós (2015) [19] | PSS1A, PSS4B | Improved modal performance index | PSS4B has greater efficiency in damping global, inter-area, and local modes compared to PSS1A. |
| Rahmatian and Seyedtabaii (2019) [24] | PSS, PSS2B | Eigenvalue stability and nonlinearity indexes | Dual-input PSS2B offers better improvements in comparison to the single-input PSS. |
| Kamwa, Grondin and Trudel (2005) [23] | PSS2B, PSS4B | - | Two type of PSSs present a similar performance in local and intra-unit, but PSS4B has better performance in inter-area mode. |
| Wang et al. (2018) [25] | PSS4B | Hybrid PSO | Two steps are used to tune parameters. |
| Peres, Júnior and Filho (2018) [26] | Simplified MB-PSS4B | Combination of different hybrid metaheuristic | Simplified structure of MB-PSS4B is used. |
| Peres, Coelho and Costa (2020) [27] | Simplified MB-PSS | Pole placement method | Simplified structure of MB-PSS is used. |
| Li, Tiong and Wong (2019) [28] | PSS4B, PSS4C | - | Optimization of PSS4C is not available. |
| Proposed work | PSS1A, OMB-PSS4C integrated IEEE Type1, ST1A | Comparison of two methods: Pattern Search and Simplex Search | A novel method is proposed to optimize MB-PSS4C under fault condition. The application of OMB-PSS4C for transient stability enhancement of power system integrated wind energy with different penetrations. |

design, parameters tuning, and superior performance. The use of MB-PSS4C has not been adequately evaluated for modern power system integrated wind energy. MB-PSS4C is considered as part of the MB stabilizer family and supersedes the MB-PSS4B model defined in IEEE recommended practice 2005 [29]. Hence, the current research is motivated by the beneficial design of MB-PSS4C and the need to address varying power system oscillations.

## III. MATERIALS AND METHODS

This section contains the overall methodology of conducting this research, and it consists of a wind farm site description and data analysis, description of PSSs and tuning optimization of MB-PSS4C. Finally, the two-area four-machine system is analysed. Fig. 1 explains the overall methodology which is used to optimize MB-PSS4C based on Simplex Search, and to enhance the transient stability of power system.

### A. SITE DESCRIPTION OF WIND FARM

Kinetic energy is absorbed from wind, transformed into a rotary motion, and converted into electricity with the aid of a generator. Wind energy is taken as stochastic energy given its continuous changes with time, with respect to wind direction and speed. Therefore, the mean speed of wind at a specific location is insufficient to determine the power generated from wind turbines. Wind speed is measured through tower placement of anemometers and in this research, the actual wind speed was taken from the Qatineh project in 2006 in Syria [30]. The maximum temperature of the site is 50 °C, and the minimum temperature is −10 °C. The average relative humidity is between 70 - 80%, and the air density is at $\rho = 1.146$ kg/m$^3$. Fig. 2 is a representation of wind speed data obtained in 2006 in every 10 minutes at the height of 40 m [30]. As observed in Fig. 2, the wind speed changes over time, it is high in June, July, and August, but the speed is low in November, December, and January.

### B. WIND DATA ANALYSIS

Wind power density at a specific area is an important parameter considered to design the wind farm. There are 2 methods of calculating the power generated by a wind turbine. The first method uses the power curve of the wind turbine, and then the second required the application of Weibull distribution [31].

The power from wind $P_{wind}$ delivered to a turbine for a wind speed V is given by equation (1) [32].

$$P_{wind} = \frac{1}{2}\rho.A.V^3 \tag{1}$$

where $\rho$ is air density in kg/m$^3$, and $A$ is swept area. Equation (2) describes the power generated by turbine [32], [33].

$$P_{out} = \frac{1}{2}\rho.A.C_P.V^3 \tag{2}$$

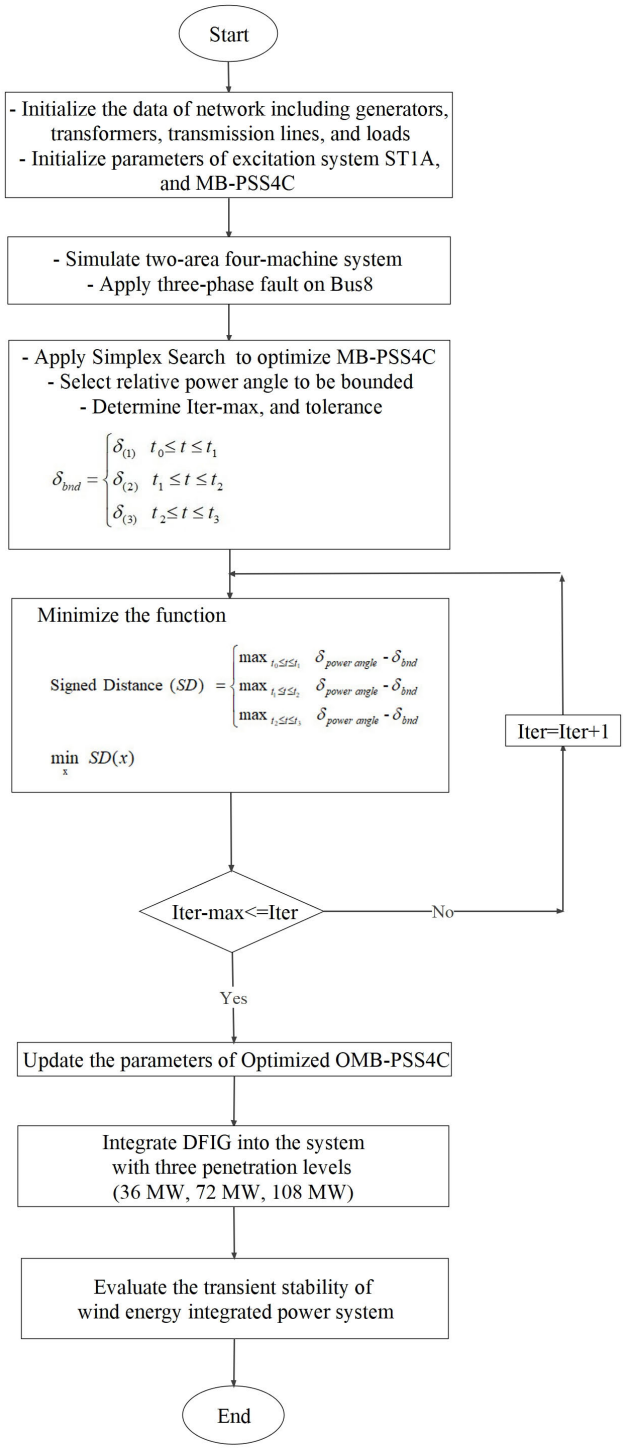


**FIGURE 1.** Flowchart used to optimize MB-PSS4C and enhance the transient stability of power system.

where $C_p$ is the power coefficient. The following equations expressed $C_p$ as functions of tip speed ratio λ and blade angle $\beta$ [32], [33].

$$C_P = f(\lambda, \beta) \tag{3}$$

$$\lambda = \frac{R * w_R}{V} \tag{4}$$

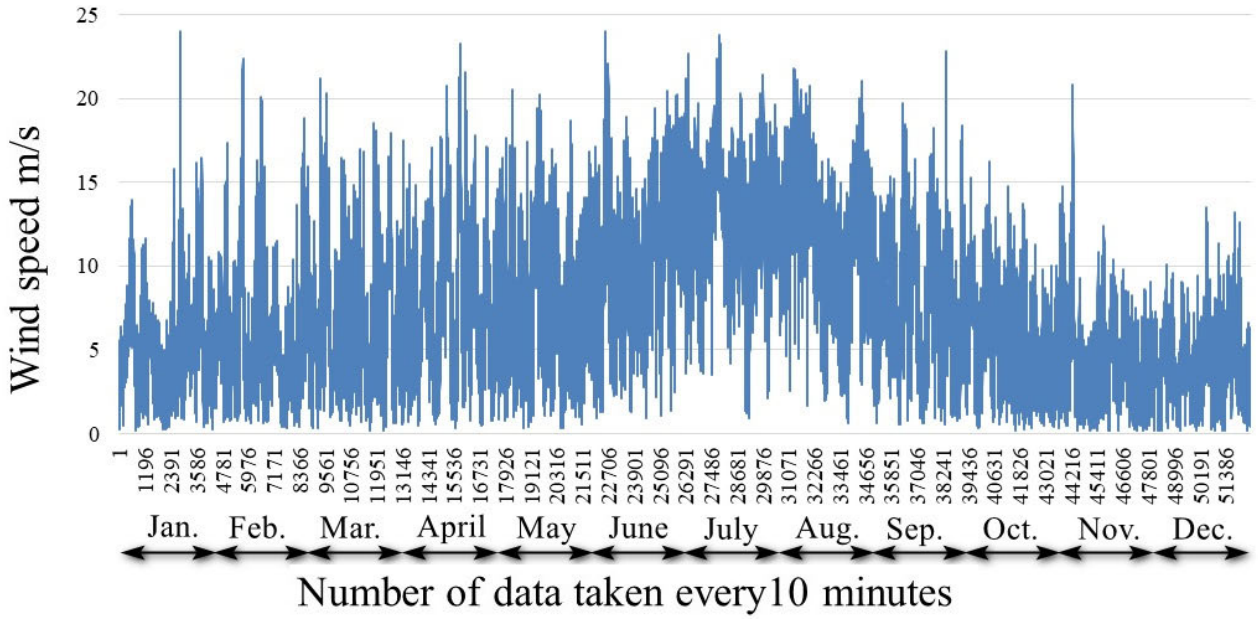


**FIGURE 2.** Yearly distribution of actual wind speed at 40 m, (wind speed data is provided by [30]).

### 1) WEIBULL DISTRIBUTION

Weibull distribution defines wind speed frequency distribution for prediction of wind power density, and its associated probability density function $f(V)$ expressed as contained in equation (5) [34], [35],

$$f(V) = \frac{k}{c}\left(\frac{V}{c}\right)^{k-1} \exp\left[-\left(\frac{V}{c}\right)^{k}\right] \tag{5}$$

where $c$ is scale parameter and $k$ is dimensionless shape parameter.

In the Standard Deviation Method (STDM). Equations (6) and (7) describe the scale and shape parameters [3].

$$k = \left(\frac{\sigma}{\overline{V}}\right)^{-1.086} \tag{6}$$

$$c = \frac{\overline{V}}{\Gamma(1+\frac{1}{k})} \tag{7}$$

where $\sigma$ is standard deviation, and $\overline{V}$ is the mean of wind speeds; $\Gamma$ is gamma function. The $\overline{V}$ and $\sigma$ are expressed as shown in equations (8) and (9), respectively [3].

$$\overline{V} = \frac{1}{N}\sum_{i=1}^{N} V_i \tag{8}$$

$$\sigma = \left[\frac{1}{N-1}\sum_{i=1}^{N}(V_i - \bar{V})^2\right]^{0.5} \tag{9}$$

where $N$ is sample data, $V_i$ is the wind speed at a specific moment, and $i$ is the measured wind speed at every 10 minutes (as considered in this research).

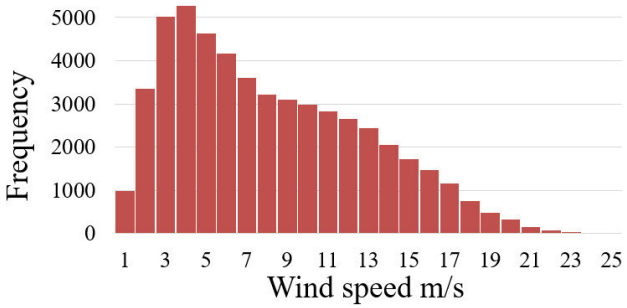


**FIGURE 3.** Histogram of observed wind data at 40 m height.

The cumulative function is the integration of Weibull distribution, and it is given by equation (10) [34], [35].

$$F(V) = 1 - \exp\left[-\left(\frac{V}{c}\right)^{k}\right] \tag{10}$$

Fig. 3 is Histogram chart representation of recorded wind speed for a period of one year at the location under investigation in this research. Fig. 4 represented the Weibull distribution and cumulative distribution functions of wind speed. As observed in Fig. 3 and Fig. 4, the Weibull distribution function shared close similarities in shape with the Histogram chart arising from the actual wind data.

### 2) WIND POWER DENSITY

The power density $P_{density}$ W/m$^2$ is expected from equation (11) [3]; the calculation was performed based on the scale and shape parameters, representing the actual wind speed data. The output power of the wind turbine $P_{out}$ is expressed in

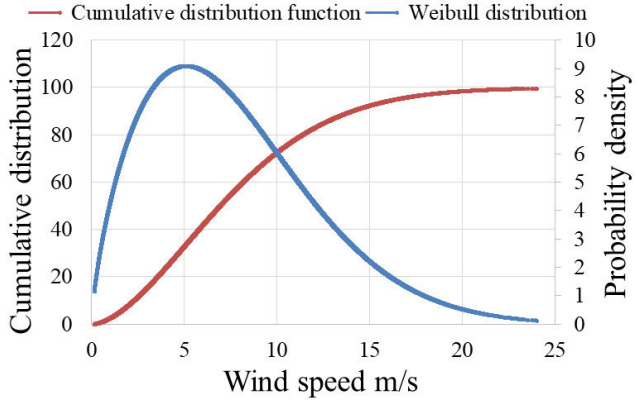


**FIGURE 4.** Probability density and cumulative distribution functions of wind speed based on Weibull distribution.

**TABLE 2.** Wind data analysis and the expected power output based on Weibull distribution.

| $\rho$ kg/m$^3$ | shape parameter | scale parameter | V m/s | $P_{density}$ W/m2 | $P_{Ele} = 0.593*P_{out}$ MW |
|---|---|---|---|---|---|
| 1.146 | 1.70 | 8.59 | 7.67 | 591.87 | 1.63 |

equation (12).

$$P_{density} = \frac{1}{2}\rho.c^3.\Gamma\left(1+\frac{3}{k}\right) \tag{11}$$

$$P_{out} = \frac{1}{2}\rho.\mathrm{A}.c^3.\Gamma\left(1+\frac{3}{k}\right) \tag{12}$$

The maximum power produced by wind turbine is equal to 59.3% of the available wind power; this value is called the Betz limit. Therefore, the electrical power $P_{Ele}$ (maximum extracted power from wind) is given as $0.593^*P_{density}{}^*A$ [3]. Table 2 is a representation of wind data analysis results based on wind speed at the investigated site.

As presented in Table 2, and based on the mathematical equations, the chosen power of DFIG for each turbine is 1.5 MW (Practically, the wind turbine is selected based on the wind characteristics and the rated power available in the market). Furthermore, the parameters of turbine and generator used in DFIG are shown in Table 3 [4], [36].

Multiple wind turbines can be installed in groups for the development of a wind farm with large electricity generation potentials. The wind farm consists of several turbines providing power for the grid. In this research, a wind farm is integrated into a power system with the capacity of each turbine $P_{Ele} = 1.5$ MW. The capacity of wind farm $P_{WF}$ is the product of the number of wind turbines $N_{WT}$ and the electrical power of each turbine $P_{Ele}$, as represented in equation (13). The number of wind turbines, for one group, is $N_{WT} = 24$ turbines (as considered in our research).

$$\begin{aligned} P_{WF} &= N_{WT} * P_{Ele} \\ P_{WF} &= 24 * 1.5 = 36\,MW \end{aligned} \tag{13}$$

**TABLE 3.** Wind energy DFIG parameters [4], [36].

| DFIG Parameters of generator, turbine, and converter components | | | |
|---|---|---|---|
| Nominal power | 1.5/0.9 MVA | Magnetizing inductance $L_m$ | 2.9 pu |
| Rated voltage | 575 V | Rated wind speed | 12 m/s |
| Frequency $f$ | 60 $Hz$ | Actual power at rated wind speed | 0.73 (pu/mechanical power) |
| Stator resistance $R_s$ | 0.00706 pu | Grid-side inductor $L_{GS}$ | 0.15 pu |
| Stator leakage inductance $L_s$ | 0.171 pu | Grid-side resistance $R_{GS}$ | 0.15/100 pu |
| Rotor resistance $R_r$ | 0.005 pu | DC link voltage | 1200 V |
| Rotor leakage inductance $L_r$ | 0.156 pu | DC capacitor | 1000 µF |

In this research, three different penetrations are considered to analyse the transient stability of wind energy integrated power system. For the first penetration, wind farm generates 36 MW (this capacity was chosen based on the wind data evaluation and pre-feasibility study for the Qatineh project). The second penetration is equal to 72 MW. Further the capacity of 108 MW is considered as high penetration of wind energy.

### C. POWER SYSTEM STABILITY

A multi-machine power system is described by using a nonlinear differential equation given by equation (14) [21].

$$\dot{x} = f(x, u) \tag{14}$$

where $x$ is the state variables and $u$ is the input variable vector including the control signal which is the input of the automatic voltage regulator [27]. The following equations represent the nonlinear dynamic model for an *ith* generator [37].

$$\frac{d\delta}{dt} = w - w_s \tag{15}$$

$$\frac{H}{\pi f}\frac{d^2\delta}{dt^2} = P_{mech} - P_e \tag{16}$$

where $\delta$ is power angle and $w$ is speed of the SG, and $ws$ is equal to $2\pi f$. $P_{mech}$ is the mechanical power, $P_e$ is the electrical power of SG. Thus, equation 16 is called a swing equation, which is used to solve the power angle of SG.

The transient voltages of SG: $E'_q$, $E'_d$, and field voltage $E_{fd}$ are given by the following equations [37], [38].

$$\frac{dE'_q}{dt} = \frac{1}{T'_{d0}}(E_{fd} - E'_q - i_d(x_d - x'_d)) \tag{17}$$

$$\frac{dE'_d}{dt} = \frac{1}{T'_{q0}}(-E'_d + i_q(x_q - x'_q)) \tag{18}$$

$$E_{fd} = \frac{1}{T_a}(-E_{fd} + K_a(V_{ref} + V_{PSS} - V_t)) \tag{19}$$

where $i_d$ and $i_q$ are the currents on d-q axes, $x_d$ and $x_q$ are the d-q reactance, $x'_d$ and $x'_q$ are the transient reactance. $T'_{d0}$ and

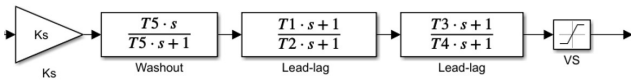


**FIGURE 5.** Single input PSS1A modelled with the use of MATLAB [17], [21].

$T'_{q0}$ are d-q axes transient open-circuit time constant. $V_{ref}$ is the reference voltage, $V_{pss}$ is the PSS output, $V_t$ is the terminal voltage.

Power system stability is affected by the type of excitation system used in the adjustment of field current and voltage regulation. In this research, 2 types of excitation systems (IEEE Type1 and ST1A) are compared to evaluate exciters' effect on power system stability. The exciter IEEE Type1 is a rotating rectifier with static voltage regulator, its parameters are taken from [39]. In contrast, ST1A is a potential-source controlled-rectifier excitation system and its parameters are selected based on IEEE Standard [40].

The relative power angles of SGs can be used in the evaluation of transient stability, like a decrease in relative power angle, is a strong indication of system stability whereas SG power angle increase, denotes an unstable system [9], [41], [42]. The power angle with respect to the reference generator is expressed as the difference between generator power angle and the reference generator power angle as contained in equation (20) [42].

$$\delta_{ij} = \delta_i - \delta_j \tag{20}$$

where $\delta_{ij}$ is the power angle of *Generator i* with respect to *Generator j*. $\delta_i$ and $\delta_j$ are the power angle of *Generator i* and *Generator j*.

#### 1) SINGLE-INPUT PSS1A

The PSS1A consists of a gain, a washout filter, 2 lead-lag filters, and a limiter. The gain defines the damping value [15], [18]. The washout filter is used in keeping the output of PSS zero under the steady-state condition [18]. At the same time, the limiter prevents the signal from exceeding the control limits. The speed deviation of the SG is the input signal of this PSS. Finally, the output of PSS is the input signal of the excitation system. The gains and time constants of PSS1A are chosen based on the type of excitation system. The parameters of PSS1A are determined based on the IEEE Standard [29]. Fig. 5 shows the PSS1A transfer functions with the single input speed deviation [17], [21].

#### 2) MULTI-BAND PSS4C

The MB-PSS4C consists of 68 parameters with multiple frequency bands, it has 2 input signals, speed deviation and electrical power of SG. The frequency bands included very-low, low, intermediate, and high-frequency modes. The very-low band be used in voltage regulation when the PSS controls a shunt compensator near the load [29]. Multi-Band PSS has a complex structure and a high number of parameters making optimization process to be very challenging. However, the high number of parameters allows more flexibility about the Optimized PSS to be operated in a large interconnected system [23]. Fig. 6 represents the diagram of MB-PSS4C with speed deviation and electrical power input signals [29]. The first lead-lag time constants for the high band mode are given by the following equations [27], [29].

$$T_{H2} = \frac{1}{2\pi * F_H * \sqrt{R}} \tag{21}$$

$$T_{H7} = T_{H2} \tag{22}$$

$$T_{H1} = \frac{T_{H2}}{R} \tag{23}$$

$$T_{H8} = R * T_{H7} \tag{24}$$

where $R$ is equal to 1.2, and $F_H$ is 9 Hz. Furthermore, it is possible to calculate the first lead-lag time constants for very-low, low, and intermediate-band modes by using equations (21) to (24) where the frequency bands are $F_{VL} = 0.01$ Hz, $F_L = 0.07$ Hz, and $F_I = 0.6$ Hz [29].

The second and third lead-lag time constants were defined as zero in the IEEE Std 421.5 [29]. In this research, the second and third lead-lag time constants are chosen in similarity to the lead-lag time constant of PSS1A. The initial values of band gains and differential filter gains are selected from IEEE Std 421.5 [29]. Then, band gains and differential filter gains are tuned based on the optimization methods, as seen in Table 4.

### D. FORMULATION OF OPTIMIZATION ALGORITHM

In this research, the optimization features are used to tune the parameters of MB-PSS4C and meet the design requirements by using MATLAB/Simulink (Response Optimization tools). The requirements are to dampen the relative power angle oscillation and decrease the settling time. The optimization methods are used to convert the requirements into a constrained problem and produce optimal parameters, within a specified tolerance, considering upper bounds. Before starting the optimization process, the relative power angle signal $\delta_{1,4}$ is selected, and upper bounds are determined. These constraints are piecewise linear bounds, and the piecewise linear bounds $\delta_{bnd}$ are represented below in equation (25) [43].

$$\delta_{bnd} = \begin{cases} \delta_{(1)} & t_0 \le t \le t_1 \\ \delta_{(2)} & t_1 \le t \le t_2 \\ \delta_{(3)} & t_2 \le t \le t_3 \end{cases} \tag{25}$$

where $\delta_{(1)}$, $\delta_{(2)}$, and $\delta_{(3)}$ are taken as the three bound sections. The simulation starts at $t_0 = 0$ s and ends at $t_3 = 10$ s. $t_1$ is the first part taken to be equal to 1.5 s, whereas the second part begins at $t_2 = 3.5$ s. The Signed Distance ($SD$) between the relative power angle and the bounds is given by equation (26) [43]. Fig. 7 shows the proposed method to determine the SDs between the power angle (before optimization) and bounds, which are specified by the user.

$$SD = \begin{cases} \max_{t_0 \le t \le t_1} & \delta_{power\ angle} - \delta_{bnd} \\ \max_{t_1 \le t \le t_2} & \delta_{power\ angle} - \delta_{bnd} \\ \max_{t_2 \le t \le t_3} & \delta_{power\ angle} - \delta_{bnd} \end{cases} \tag{26}$$

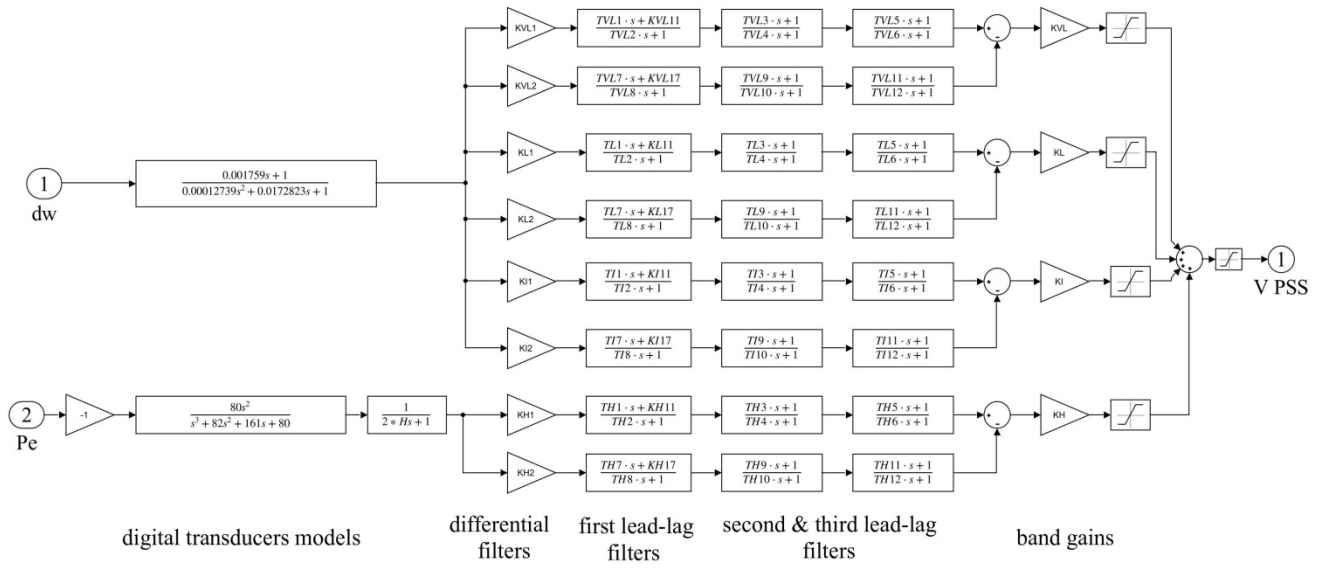


**FIGURE 6.** Diagram of MB-PSS4C with two input signals [29]. (IEEE 421.5-2016 - Reprinted and adapted with permission from IEEE. Copyright IEEE 2016. All Rights Reserved).

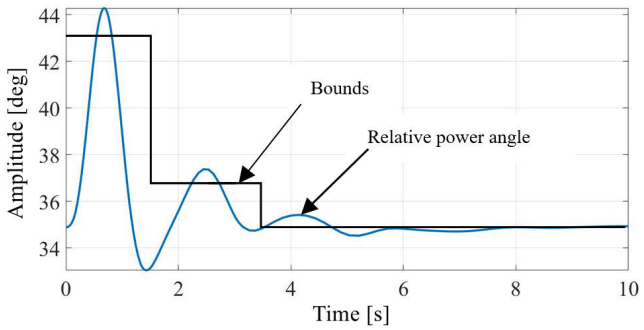


**FIGURE 7.** Signed Distance (SD) between the relative power angle of G1 and the bounds.

where $\delta_{power\ angle}$ is the simulated power angle. As observed in Fig. 7, the optimization method reduces peak power angle, settling time, and limits the signal to specific boundaries.

Several methods are used for tuning parameters in MATLAB, such as Pattern Search and Simplex Search methods. Pattern Search uses the function 'patternsearch' to optimize the parameters, and meet the requirements. While, Simplex Search uses the function 'fminsearch'. In this research, Pattern Search and Simplex Search are applied and compared to validate the optimization results and determine the suitable method for MB-PSS4C tuning parameters.

### 1) PATTERN SEARCH OPTIMIZATION METHOD

Pattern Search is a direct search to minimize a function $S(\alpha)$ of different variables. These variables are changed until the minimum value of the function is achieved [44]. Pattern Search is a derivative-free, unconstrained minimization algorithm without using the gradient or directional derivative of the objective; this method is extended to linear constrained problems [45].

The bound magnitudes of relative power angle and bound times are given, during 10 s, by equation (27). The bounds of the signal are initialized by user to reduce the settling time and peak value of relative power angle.

$$\begin{aligned} \text{Bound Magnitudes} &= [43, 43; 37, 37; 34.8, 34.8] \\ \text{Bound Times} &= [0, 1.5; 1.5, 3.5; 3.5, 10] \end{aligned} \tag{27}$$

The three bound sections are proposed to meet the optimization requirements and minimize the objective function. The simulation starts at $t_0 = 0$ s with a power angle 43° and ends at t=10 s at 34.8 power angle. The optimization problem is considered as followed (28) [45]:

$$\begin{aligned} &\min\ SD(x) \\ &\text{subject to } x_{\min} \leq Ax \leq x_{\max} \end{aligned} \tag{28}$$

where $SD(x)$ is the objective function. $Ax$ is the constraint matrix, and $x_{min}$, $x_{max}$ are the upper and lower constraints. The following constraints (29), (30), (31) are presented for high band gains to ensure that the gain limitations are chosen properly. Moreover, the same constraints are used for different band gains.

$$K_{H(\min)} < K_H < K_{H(\max)} \tag{29}$$

$$K_{H1(\min)} < K_{H1} < K_{H1(\max)} \tag{30}$$

$$K_{H2(\min)} < K_{H2} < K_{H2(\max)} \tag{31}$$

### 2) SIMPLEX SEARCH OPTIMIZATION METHOD

Simplex Search optimization method was introduced by Nelder and Mead in 1965 [46]. This method minimizes nonlinear unconstrained function $f(x)$ without derivative information; the simplex has $n$-dimensional space and $n+1$ vertices. The iteration begins by evaluating the target function for all vertices and ordering the vertices

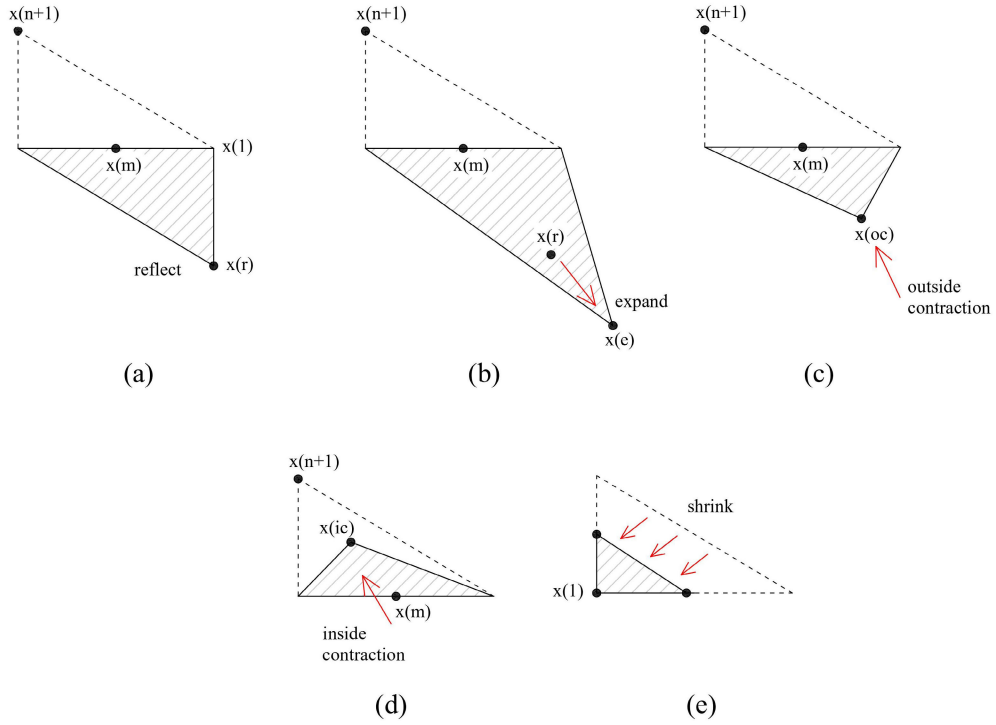


**FIGURE 8.** Simplex Search (Nelder-Mead algorithm) iteration steps, (a) Reflection, (b) Expansion, (c) Outside Contraction, (d) Inside Contraction, (e) shrink [47], [48].

$x(1), x(2), \ldots, x(n+1)$, where $f(1) < f(2) < \ldots < f(n+1)$ [47]. To minimize the target function, the worst point $x(n+1)$ and best point $x(1)$ are initialized. Then, the optimization method updates the worst and best points by the following four steps [47], [48]: reflection, expansion, contractions, and shrink, as explained in Fig. 8 [47], [48].

1) Reflection, Fig. 8 (a): in this step, a simplex reflects away $x(n+1)$ through the $x(m)$ to get a reflected point $x(r)$. Evaluate $f(1) \leq f(r) < f(n)$. If it is true, then accept the point $x(r)$ and terminate the iteration.
2) Expansion: if the new point x(r) is better than the existing best point x(1), it means: $f(r) < f(1)$. Then the simplex expands toward the new point $x(e)$, as shown in Fig. 8 (b). If $f(e) < f(r)$, accept $xe$ and terminate the iteration. Else, accept $x(r)$ and terminate the iteration.
3) Contraction is executed if $f(r) \geq f(n)$, then the simplex contracts through outside or inside contraction, as shown in Fig. 8 (c), (d).
   The outside contraction is implemented if $f(n) \leq f(r) < f(n+1)$, generate $x(oc)$, and accept $x(oc)$ if $f(oc) < f(r)$; otherwise, move to step 4.
   The inside contraction $x(ic)$ is executed if $f(r) \geq f(n+1)$. Generate and evaluate $x(ic)$. If $f(ic) < f(n+1)$, accept $x(ic)$ and end the iteration. Else, move to step 4.
4) Shrink: in this step, $n$ points are generated; the vertices of the simplex at the next iteration include the $n$ new points and the current best point $x(1)$, as presented in Fig. 8 (e).

The optimal solution of is found by doing several iterations and updating the condition of the simplex at each step. In this research, the Simplex Search is used in the optimization of MB-PSS4C towards dampening power angle oscillations and reducing settling time. This method is adopted in the tuning of MB-PSS4C since it can minimize the function without considering the constraints of variables in combination with its speedy convergence potential. The optimization requirements of this method are converted into a constrained problem for parameters tuning. The bounds of relative power angle are given by equation (32).

$$\begin{aligned} \text{Bound Magnitudes} &= [43, 43; 37, 37; 34.8, 34.8] \\ \text{Bound Times} &= [0, 1.5; 1.5, 3.5; 3.5, 10] \end{aligned} \quad (32)$$

When the requirements are met and the maximum iteration is achieved, then the solution is feasible with minimization of the problem as described in equation (33) [43], [47].

$$\min_{x} SD(x) \quad (33)$$

### *E. TWO-AREA FOUR-MACHINE MODIFIED SYSTEM*

Although the two-area four-machine system is small, it is a realistic system and an excellent example in the study of different oscillation modes [49]. The frequency of the system is 60 Hz. The system has 2 areas connected by 2 of 230 kVs' rated transmission lines and equipped with 4 generators with specific ratings of 900 MVA and 20 kV. Four transformers are utilized to step up voltage from voltage of generator

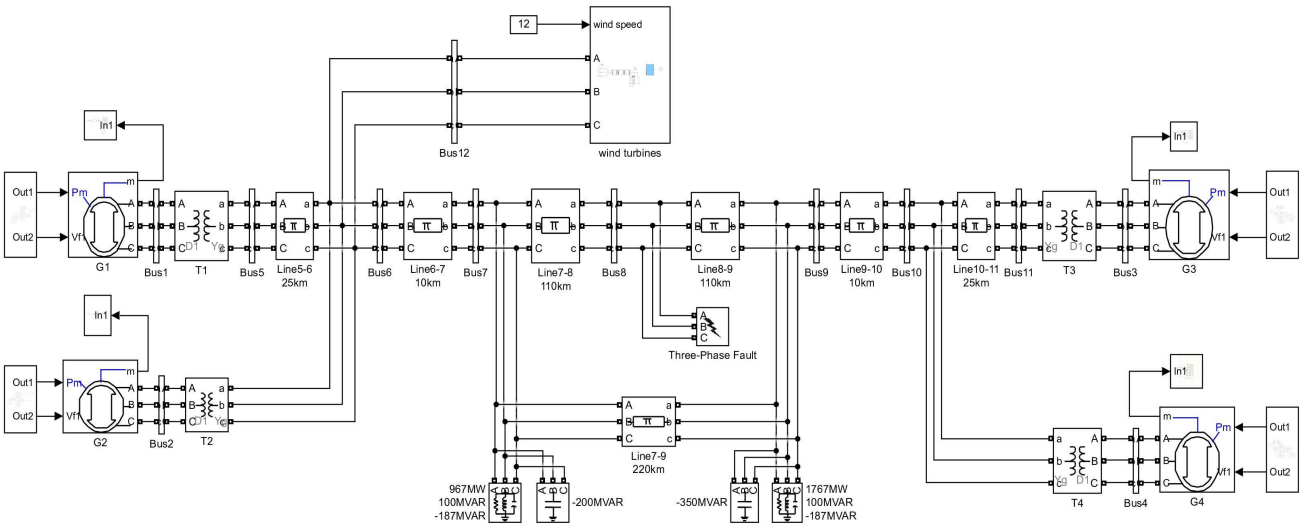


**FIGURE 9.** Two-area four-machine system integrated wind energy modelled by MATLAB software, (parameters of two-area four-machine system are found in [41], [50], [51]).

20 kV to the transmission voltage 230 kV. SGs are equipped with exciters, and the time constants and gains are chosen based on excitation system type. Generator2 is considered a swing generator, Bus2 taken as a slack bus. Generators, transmission lines, and other components data can be found in [41], [50], [51]. Fig. 9 showed the four-machine two-area system integrated wind energy and modelled with the use of MATLAB software. Whereas Fig. 10 illustrates the method used to connect PSSs and excitation systems to SG.

To study the impact of DFIG integrated into the two-area four-machine system and the advantages of using OMB-PSS4C for suppressing oscillations, a 3-phase short-circuit fault occurred at Bus8 and cleared after 200 ms. The 3-phase fault is considered as the most severe fault in electrical power system [11].

A wind farm is integrated into the system in area one [4], [22] and the impact of the wind energy with different penetrations on transient stability is comprehensively investigated. The 36 MW, 72 MW, and high penetration 108 MW are considered in this study.

## IV. RESULTS AND DISCUSSION

### A. APPLY PATTERN SEARCH AND SIMPLEX SEARCH METHODS TO TWO-AREA FOUR-MACHINE SYSTEM

In this part, the SGs are equipped with OMB-PSS4C integrated ST1A, and the two optimization methods, Pattern Search and Simplex Search, are implemented with the same number of iterations to optimize the parameters of OMB-PSS4C. The best optimization method is chosen based on the time consumed in the optimization process and its performance. The settling time and peak value of the relative power angle are used to evaluate the performance of the chosen method. The objective function, constraints, and bounds of the optimization methods were discussed in the methodology (part D).

Table 4 shows the band gains and differential filter gains of OMB-PSS4C for two-area four-machine equipped with ST1A and compares the parameters of OMB-PSS4C for Pattern Search and Simplex Search methods. Table 5 compares the Pattern Search and Simplex Search procedures for tuning the parameters of OMB-PSS4C. It also shows the time consumed in the optimization process, and the convergence characteristics for thirty iterations.

As seen in Table 5, the optimization of Simplex Search takes around 40 minutes to achieve the feasible solution for 30 iterations. However, the Pattern Search takes 165 minutes to solve the problem, and its optimization time is longer than Simplex Search. Therefore, the Simplex Search shows better results in terms of reducing the time consumed in the optimization process. Moreover, as observed in Fig. 11, the peak power angles of two methods are almost the same. While, the settling time has decreased from 7.66 s to 3 s when Simplex Search is used instead of Pattern Search. It is concluded that the Simplex Search is an effective method to optimize the parameters of OMB-PSS4C, and it is considered to optimize the parameters of PSS in this research.

### B. TRANSIENT STABILITY ANALYSIS OF THE STUDIED SYSTEM

The performance of OMB-PSS4C, based on Simplex Search, is assessed under 3-phase fault at Bus8, and the fault is cleared after 200 ms. The results show that the relative power angle $\delta_{1,4}$ has the highest value among the generators. Hence, the simulation is executed based on $G_1$ for the evaluation of transient stability of the network. The performance of PSSs is compared using the two-area four-machine system. The PSS1A with speed deviation input and OMB-PSS4C with 2 input signals are added to the excitation systems. The parameters of PSSs are chosen as explained in the

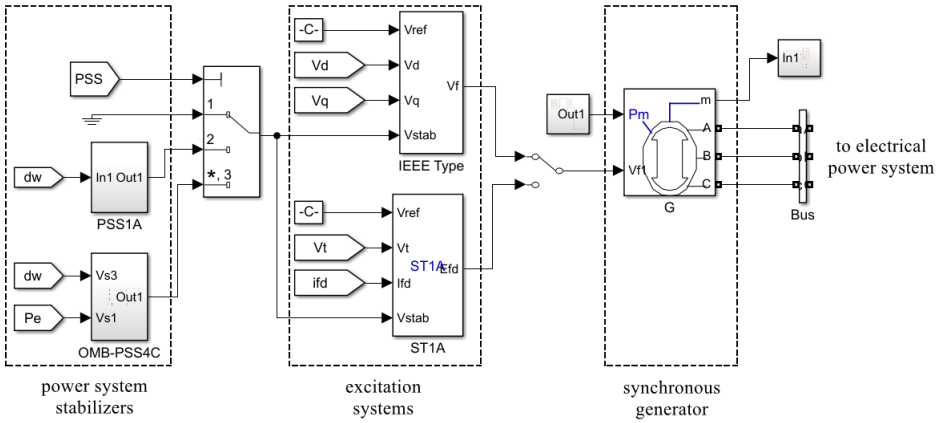


**FIGURE 10.** Power system stabilizers and excitation systems connected to a SG modelled by MATLAB.

**TABLE 4.** Band gains and differential filter gains of OMB-PSS4C connected to ST1A.

| Gain | Pattern Search | Simplex Search |
|---|---|---|
| $K_{VL}$ | 0.125 | 0.5005 |
| $K_{VL1}$ | 66 | 66.1148 |
| $K_{VL2}$ | 98 | 66.0116 |
| $K_L$ | 10 | 2.9995 |
| $K_{L1}$ | 66 | 67.6550 |
| $K_{L2}$ | 98 | 65.9857 |
| $K_I$ | 44 | 20.0008 |
| $K_{I1}$ | 66 | 67.4554 |
| $K_{I2}$ | 66 | 65.9982 |
| $K_H$ | 64 | 80.0141 |
| $K_{H1}$ | 66 | 65.9999 |
| $K_{H2}$ | 66 | 66.0012 |

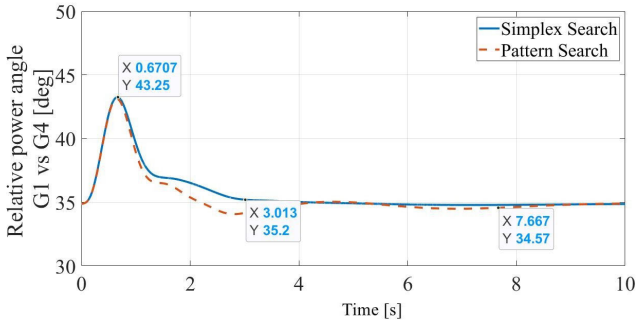


**FIGURE 11.** Relative power angle $\delta_{1,4}$ for the system integrated OMB-PSS4C with the implementation of Pattern Search and Simplex Search methods.

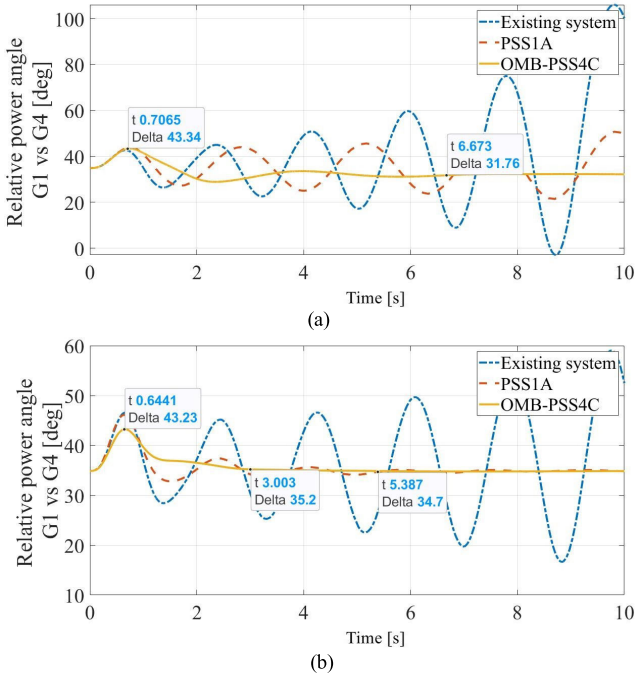


**FIGURE 12.** Relative power angle $\delta_{1,4}$ for the existing system, system with PSS1A, and system with OMB-PSS4C, a) SGs equipped with IEEE Type1, b) SGs equipped with ST1A.

methodology section of this manuscript. Fig. 12 depicts a representative plot of relative power angle ($G_1$ vs. $G_4$) for the 2 exciters and different PSSs. The power angle of the existing system oscillated during the fault, and the system became unstable, while PSSs have improved transient stability. In Fig. 12 (a), the system is stable at 6.67 s after using OMB-PSS4C integrated IEEE Type1, and the peak value is 43.34°. In Fig. 12 (b), the ST1A exciter is used, and Fig. 12 (b) shows that the system equipped with PSS1A becomes stable after 5.38 s and the peak power angle is around 46°. However, the settling time has decreased to 3 s, with 43.23° peak power angle, after adding OMB-PSS4C. Thus, the OMB-PSS4C produces a better performance when it is integrated with ST1A, unlike the IEEE Type1 exciter.

As observed in Fig. 13, the speed deviation of the system without PSS is changing over the time. On the other hand, the speed deviation is constant after 6 s on the utilization of OMB-PSS4C. Therefore, the OMB-PSS4C can return the SGs to synchronization state after clearing the fault. Moreover, Fig. 14 shows that the outputs of PSS1A and OMB-PSS4C are quite similar, and both signals are stable after 3 s. Thus, PSS only operates under the disturbance and its output is zero during the steady-state condition.

**TABLE 5. Comparison of optimization results from two different methods, pattern search and simplex search.**

| Iteration | Pattern Search method, Optimization takes 165 minutes | | Simplex Search method, Optimization takes 40 minutes | |
|---|---|---|---|---|
| | f(x) | Procedure | f(x) | Procedure |
| 1 | 0.0299312 | - | 0.0299312 | - |
| 2 | 0.0144817 | successful poll | 0.023821 | initial simplex |
| 3 | 0.0144817 | refine mesh | 0.023821 | contract outside |
| 4 | 0.0142702 | successful poll | 0.023821 | contract inside |
| 5 | 0.0142702 | refine mesh | 0.023821 | reflect |
| 6 | 0.0142702 | refine mesh | 0.023821 | reflect |
| 7 | 0.0117969 | successful poll | 0.023821 | reflect |
| 8 | 0.011791 | successful poll | 0.00851753 | shrink |
| 9 | 0.011791 | refine mesh | 0.00851753 | shrink |
| 10 | 0.011791 | refine mesh | 0.00851753 | shrink |
| 11 | 0.00855779 | successful poll | 0.00851753 | contract outside |
| 12 | 0.00843216 | successful poll | 0.00851753 | contract inside |
| 13 | 0.00843216 | refine mesh | 0.00851753 | contract outside |
| 14 | 0.00820017 | successful poll | 0.00851753 | contract inside |
| 15 | 0.00820017 | refine mesh | 0.00851753 | contract inside |
| 16 | 0.00820017 | refine mesh | 0.00851753 | contract inside |
| 17 | 0.00758845 | successful poll | 0.00851753 | contract inside |
| 18 | 0.00729544 | successful poll | 0.00851753 | contract inside |
| 19 | 0.00729544 | refine mesh | 0.00851753 | contract inside |
| 20 | 0.00729544 | refine mesh | 0.00851753 | contract inside |
| 21 | 0.00712706 | successful poll | 0.00851753 | reflect |
| 22 | 0.00712706 | refine mesh | 0.00850101 | shrink |
| 23 | 0.00703035 | successful poll | 0.00850101 | contract outside |
| 24 | 0.00699555 | successful poll | 0.00850101 | contract inside |
| 25 | 0.00699555 | refine mesh | 0.00850101 | reflect |
| 26 | 0.00699555 | refine mesh | 0.00850101 | shrink |
| 27 | 0.00699555 | refine mesh | 0.00850101 | contract inside |
| 28 | 0.00667063 | successful poll | 0.00850101 | reflect |
| 29 | 0.00667063 | refine mesh | 0.00829928 | reflect |
| 30 | 0.00659737 | successful poll | 0.00823009 | shrink |
| Settling time [s] | 7.66 s | | 3 s | |
| Peak power angle [deg] | 43.14° | | 43.25° | |

The electrical power of G1 is shown in Fig. 15. The electrical power is not constant in the existing system, but the output power remains under reasonable limits when OMB-PSS4C is used, with a slight increase in the peak value from 0.94 pu to 0.96 pu. The reason behind the improvement in electrical power of SG is that the electrical power is considered as one of the input signals of OMB-PSS4C.

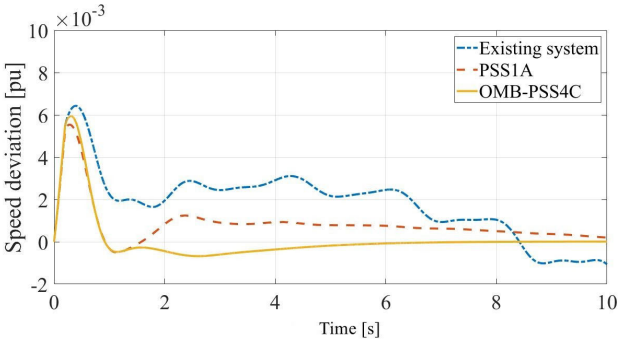


**FIGURE 13.** Speed deviation of G1 equipped with ST1A and PSSs.

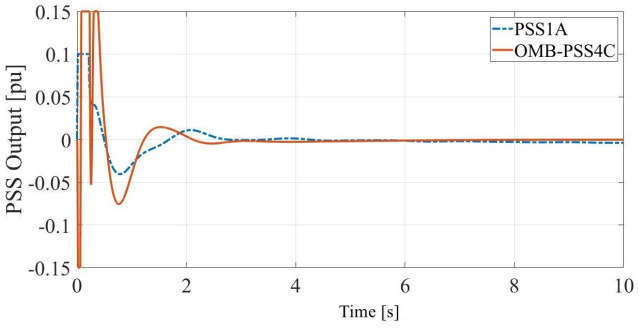


**FIGURE 14.** PSSs output of G1 equipped with ST1A.

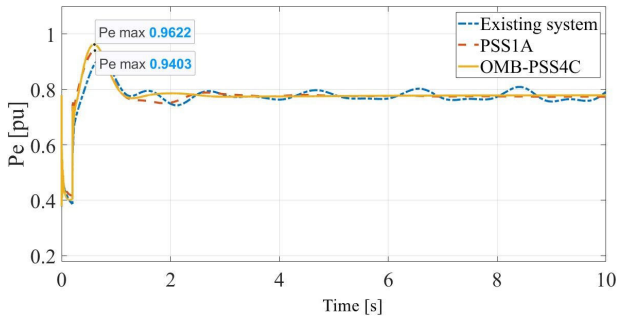


**FIGURE 15.** Electrical power of G1 equipped with ST1A and PSSs.

Fig. 16 describes the terminal voltage of G1 for the existing system and system integrated with PSSs. The voltage of G1 is not stable without PSS. But PSSs integrated excitation systems improve the voltage profile of the system, and the voltage of generators are constant after clearing the faults.

### C. TRANSIENT STABILITY ANALYSIS OF TWO-AREA FOUR-MACHINE SYSTEM INTEGRATED WITH WIND ENERGY

This section investigates the effect of different wind energy penetrations at Bus6 on the transient stability of the

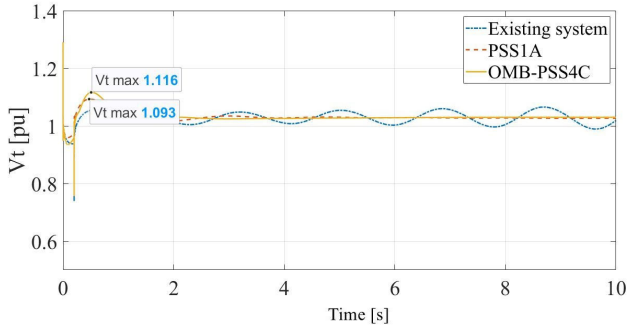


**FIGURE 16.** Terminal voltage of G1 equipped with ST1A and PSSs.

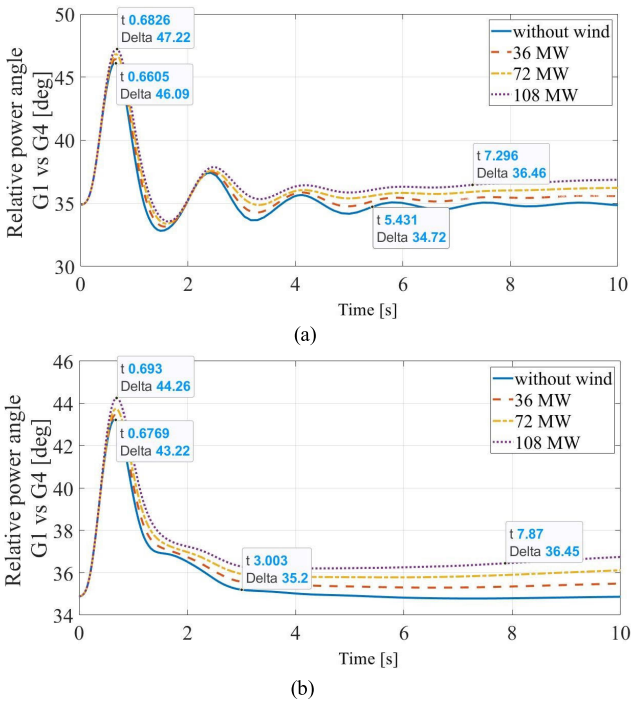


**FIGURE 17.** Relative power angle $\delta_{1,4}$ for power system integrated wind energy with different penetration levels, a) SGs equipped with PSS1A, b) SGs equipped with OMB-PSS4C.

power system. The SGs are equipped with PSS1A and OMB-PSS4C. Three different penetration levels are considered in this study, 36 MW, 72 MW, and 108 MW based wind energy. The relative power angle, the electrical power, and voltage of buses are evaluated in the following figures.

Fig. 17 presents the relative power angle of G1 for different penetrations of wind energy, and it compares the performance of PSS1A and OMB-PSS4C integrated ST1A. In Fig. 17 (a), the SGs are equipped with PSS1A. The results of relative power angle show that there is a slight increase in the peak value from 46.09 ° to 47.22° when high level of wind energy is penetrated, but the settling time has increased from 5.4 s to 7.29 s. On the other hand, as observed in Fig. 17 (b), the high penetration of wind energy increases the settling time from 3 s to 7.87 s when OMB-PSS4C is used, and the peak value of power angle is 44.26°.

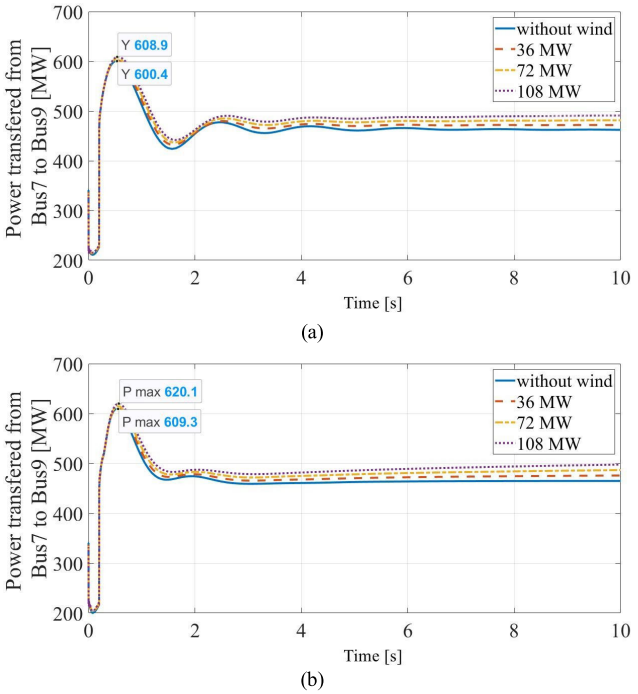


**FIGURE 18.** Power transferred from Area1 to Area2, a) SGs equipped with PSS1A, b) SGs equipped with OMB-PSS4C.

**TABLE 6.** Settling time and peak value of relative power angle of G1 vs G4 for SGs equipped with ST1A, and PSSs.

| Relative power angle | Type of PSS | System before wind energy | 36 MW wind energy | 72 MW wind energy | 108 MW wind energy |
|---|---|---|---|---|---|
| Settling time s | Existing system | Unstable | Unstable | Unstable | Unstable |
| | PSS1A | 5.4 s | 5.40 s | 6.95 s | 7.29 s |
| | OMB-PSS4C | 3 s | 2.70 s | 6.84 s | 7.87 s |
| Peak value of $\delta_{1,4}^{\circ}$ | Existing System | 54.8° | 50° | 47.04° | 47.4° |
| | PSS1A | 46.09° | 46.42° | 46.82° | 47.22° |
| | OMB-PSS4C | 43.22° | 43.46° | 43.75° | 44.26° |

The effect of different wind energy penetration on the power transferred from Area1 to Area2 is analysed in Fig. 18. The high penetration of wind energy causes an increase in the transmitted power, where the peak value has increased from 600.4 MW to 608.9 MW, and from 609.3 MW to 620.1 MW when PSS1A and OMB-PSS4C are used, respectively.

It is evident that OMB-PSS4C offers better performance than PSS1A for different penetrations of wind energy. However, the peak value of the power angle increases when more wind turbines are added to the network, and the settling time increase is equally recorded due to wind energy integration. Table 4 compares the settling time and peak value of relative power angle G1 for PSSs connected to exciter ST1A; it also includes the results of the system without PSS after integrating wind energy.

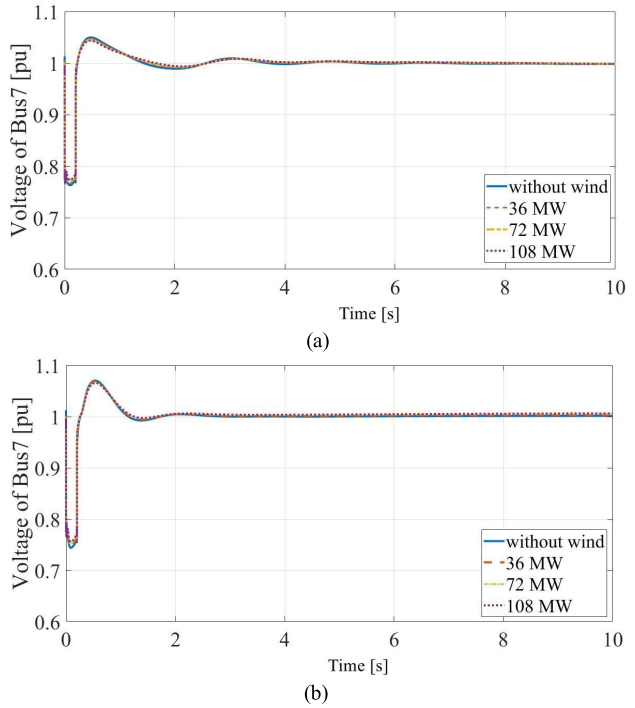


**FIGURE 19.** Voltage of Bus7, a) SGs equipped with PSS1A, b) SGs equipped with OMB-PSS4C.

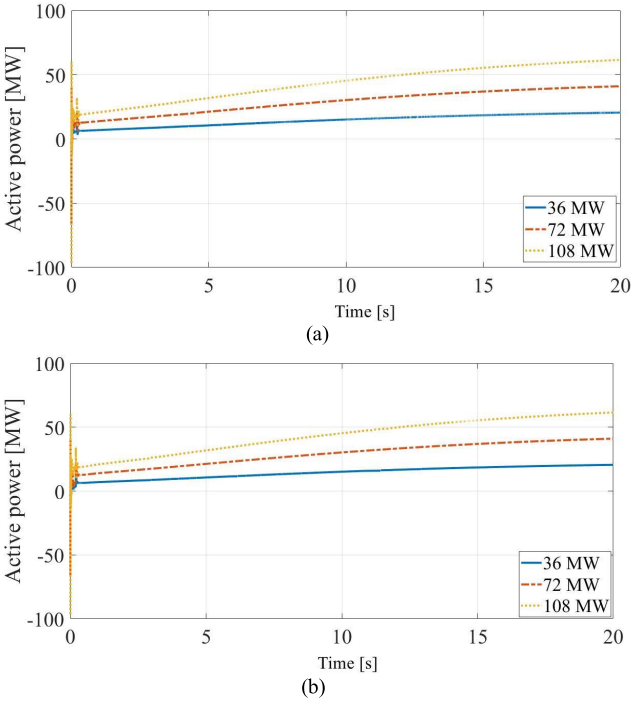


**FIGURE 20.** Active power generated by wind turbines with different penetration levels, a) SGs equipped with PSS1A, b) SGs equipped with OMB-PSS4C.

As shown in Table 6, the OMB-PSS4C improves the transient stability, and decreases the settling time and peak value with the integration of 36 MW wind energy, whereas the settling time has increased from 3 s to 7.87 s with 108 MW based wind energy.

Based on results, the OMB-PSS4C leads to significant reduction in settling time and peak value of relative power angle, and it improves the overall transient stability of wind energy integrated power system. Although, wind energy injects more power into the network and increases the power transferred from Area1 to Area2, the system remains stable when OMB-PSS4C is used.

As indicated by Fig. 19, the voltage of Bus 7 is kept constant after clearing the fault for the system with and without wind energy. Therefore, the penetration of wind energy has a negligible effect on the voltage of the strong networks.

Fig. 20 presents the active power of wind energy with different penetration levels. The output of wind energy increases when more turbines are integrated into the network. However, adding PSS to SG does not change the power generated by wind energy. Therefore, PSSs do not control the output of wind turbines. Moreover, for this fault case, the high penetration wind energy requires more than 20 s to generate the nominal power after clearing the fault, which is quite high (as shown in Fig. 20). Hence, additional control systems are recommended to control the output of wind energy with high penetration levels.

## V. CONCLUSION

In this research, the transient stability of two-area four-machine system integrated with wind energy has been effectively enhanced through the utilization of OMB-PSS4C. The parameters of OMB-PSS4C are optimized based on the Pattern Search and Simplex Search methods. The research findings include:

i. The settling time of relative power angle $\delta_{1,4}$ has decreased from 7.66 s to 3 s when the Simplex Search optimization method is implemented instead of Pattern Search.
ii. The integration of OMB-PSS4C with excitation system ST1A decreases the settling time from 6.67 s (when OMB-PSS4C integrated IEEE Type1) to 3 s. Thus, the OMB-PSS4C integrated ST1A shows a better performance compared with IEEE Type1.
iii. The high penetration levels of wind energy affect the transient stability, where the settling time has increased from 3 s to 7.87 s after 108 MW based wind energy integrated into the system.

Although this work is done by using the two-area four-machine system, but the optimization method and OMB-PSS4C controller can be applied to the actual power systems. Hence, the research findings will be beneficial for power system developers, environmental groups, and the wind energy industry operators. It also helps to drive safe penetration of wind energy systems and reduce the harmful effects of carbon emissions on the environment in modern power systems.

It is worth noting that the PSS connected to SG improves the transient stability of power systems, but it does not control the power output of wind turbines. So, the use of additional wind energy controllers or decentralized optimized

PSSs be considered as future work in the development of grid-connected wind energy.

## ACKNOWLEDGMENT

The authors gratefully acknowledge the contribution of the National Energy Research Center (NERC), Ministry of Electricity in Syrian Arab Republic, by providing wind speed data of Qatineh project.

## REFERENCES

[1] G. S. Elbasuony, S. H. E. A. Aleem, A. M. Ibrahim, and A. M. Sharaf, "A unified index for power quality evaluation in distributed generation systems," *Energy*, vol. 149, pp. 607–622, Apr. 2018, doi: 10.1016/j.energy.2018.02.088.

[2] S. S. Indira, C. A. Vaithilingam, K. S. P. Oruganti, F. Mohd, and S. Rahman, "Nanogenerators as a sustainable power source: State of art, applications, and challenges," *Nanomaterials*, vol. 9, no. 5, p. 773, May 2019, doi: 10.3390/nano9050773.

[3] A. Keyhani, M. Ghasemi-Varnamkhasti, M. Khanali, and R. Abbaszadeh, "An assessment of wind energy potential as a power generation source in the capital of Iran, Tehran," *Energy*, vol. 35, no. 1, pp. 188–201, Jan. 2010, doi: 10.1016/j.energy.2009.09.009.

[4] P. He, F. Wen, G. Ledwich, and Y. Xue, "An investigation on interarea mode oscillations of interconnected power systems with integrated wind farms," *Int. J. Electr. Power Energy Syst.*, vol. 78, pp. 148–157, Jun. 2016, doi: 10.1016/j.ijepes.2015.11.052.

[5] M. Derafshian and N. Amjady, "Optimal design of power system stabilizer for power systems including doubly fed induction generator wind turbines," *Energy*, vol. 84, pp. 1–14, May 2015, doi: 10.1016/j.energy.2015.01.115.

[6] Y.-K. Wu, T.-C. Lee, T.-Y. Hsieh, and W.-M. Lin, "Impact on critical clearing time after integrating large-scale wind power into taiwan power system," *Sustain. Energy Technol. Assessments*, vol. 16, pp. 128–136, Aug. 2016, doi: 10.1016/j.seta.2016.05.007.

[7] S. Wei, Y. Zhou, and Y. Huang, "Synchronous motor-generator pair to enhance small signal and transient stability of power system with high penetration of renewable energy," *IEEE Access*, vol. 5, pp. 11505–11512, 2017, doi: 10.1109/ACCESS.2017.2716103.

[8] S. Essallah, A. Bouallegue, and A. Khedher, "AVR and PSS controller integration in a power system: Small-signal stability study with DFIG," *IEEE/CAA J. Autom. Sinica*, vol. 1, no. 1, pp. 55–65, Jan. 2018.

[9] A. A. Alsakati, V. C. Aravind, and J. Alnasseir, "Transient stability assessment of IEEE 9-bus system integrated wind farm," in *Proc. MATEC Web Conf.*, vol. 335, 2021, p. 02006, doi: 10.1051/matecconf/202133502006.

[10] S. Xia, Q. Zhang, S. T. Hussain, B. Hong, and W. Zou, "Impacts of integration of wind farms on power system transient stability," *Appl. Sci.*, vol. 8, no. 8, p. 1289, Aug. 2018, doi: 10.3390/app8081289.

[11] M. M. Eladany, A. A. Eldesouky, and A. A. Sallam, "Power system transient stability: An algorithm for assessment and enhancement based on catastrophe theory and FACTS devices," *IEEE Access*, vol. 6, pp. 26424–26437, 2018, doi: 10.1109/ACCESS.2018.2834906.

[12] D. Chatterjee and A. Ghosh, "Improvement of transient stability of power systems with STATCOM-controller using trajectory sensitivity," *Int. J. Electr. Power Energy Syst.*, vol. 33, no. 3, pp. 531–539, Mar. 2011, doi: 10.1016/j.ijepes.2010.12.005.

[13] L. Wang and D.-N. Truong, "Stability enhancement of DFIG-based offshore wind farm fed to a multi-machine system using a STATCOM," *IEEE Trans. Power Syst.*, vol. 28, no. 3, pp. 2882–2889, Aug. 2013, doi: 10.1109/TPWRS.2013.2248173.

[14] J. Bhukya and V. Mahajan, "Optimization of controllers parameters for damping local area oscillation to enhance the stability of an interconnected system with wind farm," *Int. J. Electr. Power Energy Syst.*, vol. 119, Jul. 2020, Art. no. 105877, doi: 10.1016/j.ijepes.2020.105877.

[15] M. Edrah, K. L. Lo, and O. Anaya-Lara, "Impacts of high penetration of DFIG wind turbines on rotor angle stability of power systems," *IEEE Trans. Sustain. Energy*, vol. 6, no. 3, pp. 759–766, Jul. 2015, doi: 10.1109/TSTE.2015.2412176.

[16] X. Y. Bian, Y. Geng, K. L. Lo, Y. Fu, and Q. B. Zhou, "Coordination of PSSs and SVC damping controller to improve probabilistic small-signal stability of power system with wind farm integration," *IEEE Trans. Power Syst.*, vol. 31, no. 3, pp. 2371–2382, May 2016, doi: 10.1109/TPWRS.2015.2458980.

[17] J. Bhukya and V. Mahajan, "Optimization of damping controller for PSS and SSSC to improve stability of interconnected system with DFIG based wind farm," *Int. J. Electr. Power Energy Syst.*, vol. 108, pp. 314–335, Jun. 2019, doi: 10.1016/j.ijepes.2019.01.017.

[18] T. Surinkaew and I. Ngamroo, "Coordinated robust control of DFIG wind turbine and PSS for stabilization of power oscillations considering system uncertainties," *IEEE Trans. Sustain. Energy*, vol. 5, no. 3, pp. 823–833, Jul. 2014, doi: 10.1109/TSTE.2014.2308358.

[19] D. Rimorov, I. Kamwa, and G. Joós, "Model-based tuning approach for multi-band power system stabilisers PSS4B using an improved modal performance index," *IET Gener., Transmiss. Distrib.*, vol. 9, no. 15, pp. 2135–2143, Nov. 2015, doi: 10.1049/iet-gtd.2014.1176.

[20] T. Hussein, M. S. Saad, A. L. Elshafei, and A. Bahgat, "Damping interarea modes of oscillation using an adaptive fuzzy power system stabilizer," *Electr. Power Syst. Res.*, vol. 80, no. 12, pp. 1428–1436, Dec. 2010, doi: 10.1016/j.epsr.2010.06.004.

[21] A. Khodabakhshian, R. Hemmati, and M. Moazzami, "Multi-band power system stabilizer design by using CPCE algorithm for multi-machine power system," *Electr. Power Syst. Res.*, vol. 101, pp. 36–48, Aug. 2013, doi: 10.1016/j.epsr.2013.03.011.

[22] P. R. Nakhi and M. A. Kamarposhti, "Multi objective design of type II fuzzy based power system stabilizer for power system with wind farm turbine considering uncertainty," *Int. Trans. Electr. Energy Syst.*, vol. 30, no. 4, p. e12285, Apr. 2020.

[23] I. Kamwa, R. Grondin, and G. Trudel, "IEEE PSS2B versus PSS4B: The limits of performance of modern power system stabilizers," *IEEE Trans. Power Syst.*, vol. 20, no. 2, pp. 903–915, May 2005, doi: 10.1109/TPWRS.2005.846197.

[24] M. Rahmatian and S. Seyedtabaii, "Multi-machine optimal power system stabilizers design based on system stability and nonlinearity indices using hyper-spherical search method," *Int. J. Electr. Power Energy Syst.*, vol. 105, pp. 729–740, Feb. 2019, doi: 10.1016/j.ijepes.2018.09.024.

[25] D. Wang, N. Ma, M. Wei, and Y. Liu, "Parameters tuning of power system stabilizer PSS4B using hybrid particle swarm optimization algorithm," *Int. Trans. Electr. Energy Syst.*, vol. 28, no. 9, p. e2598, Sep. 2018, doi: 10.1002/etep.2598.

[26] W. Peres, I. C. S. Júnior, and J. A. P. Filho, "Gradient based hybrid metaheuristics for robust tuning of power system stabilizers," *Int. J. Electr. Power Energy Syst.*, vol. 95, pp. 47–72, Feb. 2018, doi: 10.1016/j.ijepes.2017.08.014.

[27] W. Peres, F. C. R. Coelho, and J. N. N. Costa, "A pole placement approach for multi-band power system stabilizer tuning," *Int. Trans. Electr. Energy Syst.*, vol. 30, no. 10, p. e12548, Oct. 2020, doi: 10.1002/2050-7038.12548.

[28] Z. Li, T. Tiong, and K. Wong, "Transient stability improvement by using PSS4C in hybrid PV wind power system," in *Proc. 1st Int. Conf. Electr., Control Instrum. Eng. (ICECIE)*, Kuala Lumpur, Malaysia, Nov. 2019, pp. 1–6, doi: 10.1109/ICECIE47765.2019.8974751.

[29] *IEEE Recommended Practice for Excitation System Models for Power System Stability Studies*, IEEE Standard 421.5 (Revision IEEE Std 421.5-2005), Aug. 2016, p. 207, doi: 10.1109/IEEESTD.2016.7553421.

[30] *Qatineh Pilot Project Wind Park*, Nat. Energy Res. Centre, Ministry Electr., New Delhi, India, 2011.

[31] A. Azad, M. Rasul, and T. Yusaf, "Statistical diagnosis of the best Weibull methods for wind power assessment for agricultural applications," *Energies*, vol. 7, no. 5, pp. 3056–3085, May 2014, doi: 10.3390/en7053056.

[32] C. Aravind, R. Rajparthiban, R. Rajprasad, I. Grace, R. Teymourzadeh, and M. Norhisam, "Mathematical toolbox and its application in the development of laboratory scale vertical axis wind turbine," in *Proc. IEEE Int. Conf. Power Energy (PECon)*, Dec. 2012, pp. 99–104.

[33] C. V. Aravind, R. Rajparthiban, R. Rajprasad, and Y. V. Wong, "A novel magnetic levitation assisted vertical axis wind turbine—Design procedure and analysis," in *Proc. IEEE 8th Int. Colloq. Signal Process. Appl.*, Malacca, Malaysia, Mar. 2012, pp. 93–98, doi: 10.1109/CSPA.2012.6194698.

[34] J. V. Seguro and T. W. Lambert, "Modern estimation of the parameters of the Weibull wind speed distribution for wind energy analysis," *J. Wind Eng. Ind. Aerodyn.*, vol. 85, no. 1, pp. 75–84, Mar. 2000, doi: 10.1016/S0167-6105(99)00122-1.

[35] S. A. Akdağ and A. Dinler, "A new method to estimate Weibull parameters for wind energy applications," *Energy Convers. Manage.*, vol. 50, no. 7, pp. 1761–1766, Jul. 2009, doi: 10.1016/j.enconman.2009.03.020.

[36] M. Soliman, O. P. Malik, and D. T. Westwick, "Multiple model predictive control for wind turbines with doubly fed induction generators," *IEEE Trans. Sustain. Energy*, vol. 2, no. 3, pp. 215–225, Jul. 2011, doi: 10.1109/TSTE.2011.2153217.
[37] S. Mishra, M. Tripathy, and J. Nanda, "Multi-machine power system stabilizer design by rule based bacteria foraging," *Electr. Power Syst. Res.*, vol. 77, no. 12, pp. 1595–1607, Oct. 2007, doi: 10.1016/j.epsr.2006.11.006.
[38] D. Butti, S. K. Mangipudi, and S. R. Rayapudi, "An improved whale optimization algorithm for the design of multi-machine power system stabilizer," *Int. Trans. Electr. Energy Syst.*, vol. 30, no. 5, p. e12314, May 2020, doi: 10.1002/2050-7038.12314.
[39] I. Report, "Excitation system models for power system stability studies," *IEEE Trans. Power App. Syst.*, vol. PAS-100, no. 2, pp. 494–509, Feb. 1981, doi: 10.1109/TPAS.1981.316906.
[40] *IEEE Recommended Practice for Excitation System Models for Power System Stability Studies*, IEEE Standard 421.5TM, (Revision IEEE Std 421.5-1992), 2005, p. 95, doi: 10.1109/IEEESTD.2006.99499.
[41] P. Kundur, N. J. Balu, and M. G. Lauby, *Power System Stability and Control*. New York, NY, USA: McGraw-Hill, 1994.
[42] P. M. Anderson and A. A. Fouad, *Power System Control and Stability*, 2nd ed. Hoboken, NJ, USA: Wiley, 2003.
[43] MathWorks, Help Center. *How the Optimization Algorithm Formulates Minimization Problems—MATLAB & Simulink*. Accessed: Nov. 26, 2020. [Online]. Available: https://www.mathworks.com/help/sldo/ug/how-the-optimization-algorithm-formulates-minimization-problems.html
[44] R. Hooke and T. A. Jeeves, "'Direct search' solution of numerical and statistical problems," *J. ACM*, vol. 8, no. 2, pp. 212–229, Apr. 1961, doi: 10.1145/321062.321069.
[45] R. M. Lewis and V. Torczon, "Pattern search methods for linearly constrained minimization," *SIAM J. Optim.*, vol. 10, no. 3, pp. 917–941, Jan. 2000, doi: 10.1137/s1052623497331373.
[46] J. A. Nelder and R. Mead, "A simplex method for function minimization," *Comput. J.*, vol. 7, no. 4, pp. 308–313, Jan. 1965, doi: 10.1093/comjnl/7.4.308.
[47] J. C. Lagarias, J. A. Reeds, M. H. Wright, and P. E. Wright, "Convergence properties of the nelder-mead simplex method in low dimensions," *SIAM J. Optim.*, vol. 9, no. 1, pp. 112–147, Jan. 1998, doi: 10.1137/S1052623496303470.
[48] R. Barati, "Parameter estimation of nonlinear muskingum models using nelder-mead simplex algorithm," *J. Hydrol. Eng.*, vol. 16, no. 11, pp. 946–954, Nov. 2011, doi: 10.1061/(ASCE)HE.1943-5584.0000379.
[49] W. Peres, "Multi-band power oscillation damping controller for power system supported by static VAR compensator," *Electr. Eng.*, vol. 101, no. 3, pp. 943–967, Sep. 2019, doi: 10.1007/s00202-019-00830-9.
[50] I. Kamwa. *(Hydro-Quebec) Performance of Three PSS for Interarea Oscillations—MATLAB & Simulink*. Accessed: Oct. 26, 2020. [Online]. Available: https://www.mathworks.com/help/physmod/sps/ug/performance-of-three-pss-for-interarea-oscillations.html
[51] Z. A. Obaid, M. T. Muhssin, and L. M. Cipcigan, "A model reference-based adaptive PSS4B stabilizer for the multi-machines power system," *Electr. Eng.*, vol. 102, no. 1, pp. 349–358, Mar. 2020, doi: 10.1007/s00202-019-00879-6.

**AHMAD ADEL ALSAKATI** (Student Member, IEEE) received the B.Eng. degree in electrical engineering and the master's degree in electrical power systems engineering from Damascus University, Syria, in 2007 and 2012, respectively. He is currently pursuing the Ph.D. degree with the School of Computer Science and Engineering, Taylor's University. His research interests include electrical power system operating, planning, and optimization. He also focuses on renewable energy integration power systems and the impact of distributed generation on power system stability. He is a member of the IEEE Power and Energy Society (PES).

**CHOCKALINGAM ARAVIND VAITHILINGAM** (Senior Member, IEEE) received the B.Eng. degree from Bharathiyar University, India, in 1998, the M.Eng. degree from Bharathidasan University, India, in 2001, and the Ph.D. degree in electrical power engineering from Universiti Putra Malaysia, in 2013. He is heading the Electrical and Electronic Engineering Program, Faculty of Innovation and Technology, Taylor's University, Malaysia, and heading the research cluster VERTICALS aligned with SDG goals on sustainable energy and mobility (SDG 7, 11). He is currently a very frequent speaker at various international and national platforms. He is also a Professional Technologists with the Malaysian Board of Technologists. He is a member of IET, U.K., and the Society of Engineering Education Malaysia. He is also a registered Chartered Engineer registered professional with the Engineering Council, U.K.

**JAMAL ALNASSEIR** received the B.Sc. degree in electrical engineering from Damascus University, Syria, in 1994, the Diploma degree in power system, in 1996, the master's degree in high voltage, in 2000, and the Ph.D. degree in electrical engineering from the University of Erlangen-Nuermberg, Germany, in 2007. He is currently an Associated Professor with the Electric Power Engineering Department, Damascus University. His research interests include high voltage technology, power electronic, renewable energy sources, transient stability, and electrical networks.

**ARTHANARI JAGADEESHWARAN** (Member, IEEE) is currently associated with the Department of Electrical and Electronics Engineering, Sona College of Technology, India. He has about 22 years of academic experience which includes 14 years in research and development. He has published over 30 indexed journals in the field of special electrical machines, power quality, and control electronics. His prime interests include renewable energy systems, and development of permanent magnet motors and drives for special purpose and aerospace applications. He is a member of ISSE and IE.